European Journal of Medicinal Chemistry 48 (2012) 284–295

Contents lists available at SciVerse ScienceDirect

European Journal of Medicinal Chemistry

journal homepage: http://www.elsevier.com/locate/ejmech

Original article

Synthesis and biological assessment of novel 2-thiazolylhydrazones and computational analysis of their recognition by monoamine oxidase B

Simona Distinto [a], Matilde Yáñez [b], Stefano Alcaro [a,*], M. Cristina Cardia [c], Marco Gaspari [d], M. Luisa Sanna [c], Rita Meleddu [c], Francesco Ortuso [a], Johannes Kirchmair [e], Patrick Markt [e], Adriana Bolasco [f], Gerhard Wolber [g], Daniela Secci [f], Elias Maccioni [c]

[a] Dipartimento di Scienze della Salute, Università degli Studi "Magna Græcia" di Catanzaro, Campus "Salvatore Venuta", Viale Europa, 88100 Catanzaro (CZ), Italy
[b] Departamento de Farmacología and Instituto de Farmacia Industrial, Universidad de Santiago de Compostela, Campus Universitario Sur, E-15782 Santiago de Compostela, Spain
[c] Dipartimento Farmaco Chimico Tecnologico, University of Cagliari, Via Ospedale 72, 09124 Cagliari, Italy
[d] Dipartimento di Medicina Sperimentale e Clinica, Università degli Studi "Magna Græcia" di Catanzaro, Campus "Salvatore Venuta", Viale Europa, 88100 Catanzaro (CZ), Italy
[e] Department of Pharmaceutical Chemistry, University of Innsbruck, Innrain 52c, A-6020 Innsbruck, Austria
[f] Dipartimento di Studi di Chimica e Tecnologia delle Sostanze Biologicamente Attive, University "La Sapienza" of Rome, P.le A. Moro 5, 00185 Rome, Italy
[g] Department of Pharmaceutical Chemistry, University "Freie" of Berlin, Königin-Luise-Str. 2, 14195 Berlin, Germany

ARTICLE INFO

Article history:
Received 2 March 2011
Received in revised form
25 November 2011
Accepted 18 December 2011
Available online 24 December 2011

Keywords:
FEP
GRID
Induced fit docking
MAO-B inhibitors
Molecular dynamics

ABSTRACT

Monoamine oxidase B (MAO-B) is a promising target for the treatment of neurodegenerative disorders. We report the synthesis and the biological evaluation of halogenated derivatives of 1-aryliden-2-(4-phenylthiazol-2-yl)hydrazines. The fluorinated series shows interesting activity and great selectivity toward the human recombinant MAO-B isoform expressed in baculovirus infected BTI insect cells. The multiple crystal structures alignment of the enzyme highlighted pronounced induced fit (IF) adaptations with respect to bound ligands. Therefore, IF docking (IFD) experiments and molecular dynamic (MD) simulations were carried out to reveal the putative binding mode and to explain the experimentally observed differences in the activity of 1-(aryliden-2-(4-(4-chlorophenyl)thiazol-2-yl)hydrazines. The importance of water molecules within the binding site was also investigated. These are known to play an important role in the binding site cavity and to mediate protein–ligand interactions. Detailed analyses of the trajectories provide insights on the chemical features required for the activity of this scaffold. In particular it was highlighted the importance of fluorine atom interacting with the water close to the cofactor and the influence of steric bulkiness of substituents in the arylidene moiety. Free energy perturbation (FEP) analysis confirmed experimental data. The information we deduced will help to develop novel high-affinity MAO-B inhibitors.

1. Introduction

It is common knowledge that both isoforms of monoamine oxidase, A and B, (MAO, EC 1.4.3.4), play a key role in the metabolism of neurotransmitters and are important targets for the treatment of psychiatric and neurological diseases. In particular, the relevance of MAO-B in the pathogenesis of Parkinson's disease (PD) and the therapeutic potential of MAO-B selective inhibitors in this pathology has been pointed out [1,2]. Moreover, the interest toward the B isoform of MAO has grown since the detection of increased MAO-B levels in a number of neurodegenerative disorders such as Alzheimer's disease, Huntington's chorea, and amyotrophic lateral sclerosis [3,4].

Thus, MAO-B inhibitors are considered promising agents for the treatment of several neurodegenerative disorders. Selegiline [*R*-(−)-deprenyl], an irreversible MAO-B inhibitor has been used in combination with *l*-Dopa for PD treatment for some time. Evidence on the effect of slowing down the progression of PD suggests these inhibitors could be useful therapeutic agents in the early stages of the disease. Recently, rasagiline, (*N*-propargyl-1-*R*-aminoindan, Azilect), a novel selective and irreversible MAO-B inhibitor, has been approved for PD therapy [5] while safinamide, a selective and reversible MAO-B inhibitor, is currently undergoing clinical phase III for the treatment of early stages of PD [6].

On this basis, we focused our interest on the design of potential MAO-B inhibitors. We have recently reported the synthesis and the

* Corresponding author. Tel.: +39 0961 3694197; fax: +39 0961 515509.
E-mail address: alcaro@unicz.it (S. Alcaro).

0223-5234/$ – see front matter © 2011 Elsevier Masson SAS. All rights reserved.
doi:10.1016/j.ejmech.2011.12.027

biological activity of a series of 2-thiazolylhydrazones [7]. Encouraged by these results we have synthesized and studied a new series of 1-arylidene-2-(4-arylthiazol-2-yl)hydrazines to investigate the influence of the introduction of 4-chloro- or 4-fluoro-phenyl moiety in the position four of the thiazole ring. The importance of fluorine in medicinal chemistry is well recognized and discussed extensively in literature [8,9]. The introduction of fluorine causes modulation of electronic, lipophilic, and steric parameters, which determine pharmacodynamic and pharmacokinetic properties and may also influence biological activity. In our study, fluorine seems to play a pivotal role for both activity and selectivity toward the B isoform.

In recent years, thanks to the availability of several crystal structures, the mechanism and the basis of selective inhibition of MAO-B has become clearer. A requirement that seems to be important for selectivity is the ability of the inhibitors to fit within both substrate and entrance cavity; since the elongated bipartite cavity of MAO-B is bigger (700 $Å^3$) than the single round substrate cavity of MAO-A (550 $Å^3$) [10,11]. Rational drug design relies on *in silico* methods. Their application is growing rapidly in both academia and industry, as such methods allow for increasing lead retrieval rates and understanding the molecular mechanism of action of known and new active compounds [12].

Several computational studies on this target have been published and help by elucidating the activity of different series of compounds [13–16]. Is it known that small modifications on small molecules may lead to different activity or target selectivity [17,18]. In order to better understand the differences in activity of this series of synthesized compounds, where fluorine was substituted by isosteric chlorine, IFD experiments of the two series have been carried out and followed by MD simulations for the most active 4-fluorophenyl derivative, **5a**, and the homologous 4-chlorophenyl compound **5b**. Moreover, to confirm experimental data we have performed FEP analysis.

2. Chemistry and biochemistry

The synthetic procedure for the preparation of the novel 2-thiazolylhydrazone derivatives (**1**–**6**)**a** and (**1**–**6**)**b** was performed as reported in our previous communication [7]. The appropriate aryl aldehydes react directly with thiosemicarbazide, and the obtained thiosemicarbazones react either with 2-bromo-4′-chloroacetophenone or 2-chloro-4′-fluoroacetophenone to give the 4-substituted thiazole ring derivatives (Scheme 1).

All reactions were performed using isopropyl alcohol as solvent and were monitored by TLC analysis. The obtained reaction products (**1**–**6**)**a** and (**1**–**6**)**b** precipitated upon cooling, and were filtered and purified by crystallization from ethanol or ethanol/isopropanol. All the synthesized products have been characterized by analytical and spectroscopic methods (see Experimental section).

The hMAO activity was evaluated with microsomal MAO isoforms prepared from insect cells (BTI-TN-5B1-4) infected with recombinant baculovirus containing cDNA inserts for hMAO-A or hMAO-B and following the general procedure (see Experimental section) [19]. The tested drugs (new compounds and reference inhibitors) inhibited the control enzymatic MAO activities and the inhibition was concentration-dependent. The corresponding IC_{50} values are shown in Table 1.

3. Computational methods

Several computational methods were applied on three levels to gain insight about: i) structure of the enzyme; ii) molecular recognition; iii) free energy evaluation of complexes (Table 2).

3.1. Structure alignment

The starting geometries for the MD simulations were acquired by means of docking the compounds into the MAO-B active site. Several X-ray structures co-crystallized with different MAO-B inhibitors are available from the Protein Data Bank (PDB) [20]. With the purpose to identify differences in the binding mode and to gain knowledge on the conserved waters within the binding pocket, we aligned twenty complexes with resolution better than 2.5 Å and without mutations (PDB codes: 2byb, 2bk3, 2c64, 2c65, 2c66, 2c67, 2c70, 1oj9, 1oja, 1ojb, 1ojc, 1s2q, 1s2y, 1s3b, 1s3e, 2v5z, 2v60, 2v61, 2vrm, 2vrl). The 3D-structures and the sequences of crystallized complexes were aligned with MOE-Align [21] (Fig. 1).

The alignment revealed that, while most of the residues in the substrate cavity are almost perfectly superimposed and are characterized by low b-factor values, the residues of the access cavity are quite flexible (e.g. AA 99-105, Tyr326, Ile199, Phe118, Trp119).

3.2. Structural water

Nine water molecules within a 4.5 Å distance range radius from the crystallized ligands, conserved in the investigated PDB

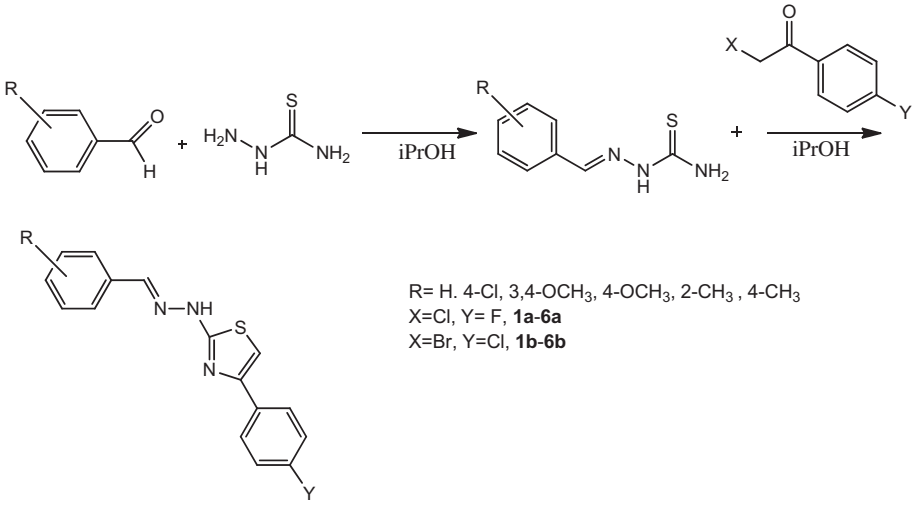

Scheme 1. Synthetic pathway to compounds **1a**–**6a**, **1b**–**6b**.

Table 1
IC_{50} values for the inhibitory effects of test drugs (new compounds and reference inhibitors) on the enzymatic activity of human recombinant MAO isoforms expressed in baculovirus infected BTI insect cells.

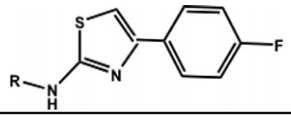

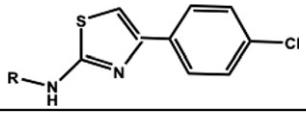

Compounds	R	MAO-A (IC_{50})	MAO-B (IC_{50})(μM)	Compounds	R	MAO-A (IC_{50})	MAO-B (IC_{50}))(μM)
1a	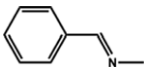	***	0.79 ± 0.04	**1b**	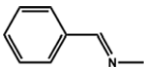	***	***
2a	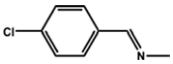	***	1.32 ± 0.05	**2b**	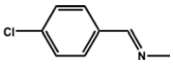	***	***
3a	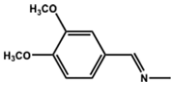	***	2.39 ± 0.10	**3b**	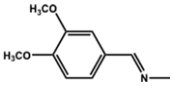	***	***
4a	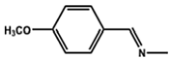	***	9.24 ± 0.36	**4b**	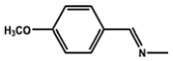	***	***
5a	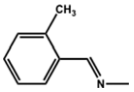	***	0.19 ± 0.01	**5b**	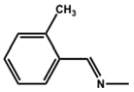	***	***
6a	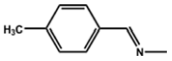	**	44.74 ± 1.68	**6b**	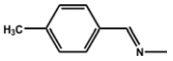	**	***

Drugs	Structure	MAO-A (IC_{50})(μM)	MAO-B (IC_{50})(μM)	Drugs	Structure	MAO-A (IC_{50})(μM)	MAO-B (IC_{50})(μM)
Clorgyline	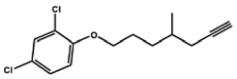	0.0046 ± 0.0003[a]	61.35 ± 1.13	Iproniazide	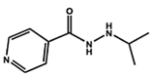	6.56 ± 0.76	7.54 ± 0.36
Deprenyl	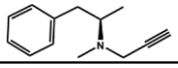	67.25 ± 1.02[a]	0.019 ± 0.00086	Moclobemide	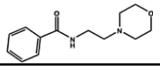	361.38 ± 19.37	*

All IC_{50} values shown in this table are the mean ± S.E.M. from five experiments.
* Inactive at 1 mM (highest concentration tested).
** Inactive at 100 μM (highest concentration tested). At higher concentration the compounds precipitate.
*** 100 μM inhibits the corresponding MAO activity by approximately 40–45%. At higher concentration the compounds precipitate.
[a] Level of statistical significance: $P < 0.01$ *versus* the corresponding IC_{50} values obtained against MAO-B, as determined by ANOVA/Dunnett's.

complexes, have been identified. These are likely to be important for mediating interactions of inhibitors and were therefore taken into account in the docking experiments. In fact, several studies have highlighted the importance of water bound to residues in the binding pocket in numerous proteins [22,23]. Previous docking studies have already pointed out the impact of water molecules in proximity of the MAO-B flavin adenine dinucleotide (FAD) cofactor [24–26] and recent crystallization studies have shown their role in recognition and stabilization of the interaction between the ligand and its binding site [11,27]. To estimate the significance of these

Table 2
Computational approaches applied.

	Approach	Program	Aim
i) Structure analysis	- Structure alignment PDB models	MOE alignment	Investigation of flexible areas.
	- Structural water study	GRID analysis with OH2 probe	Analysis of energetic favorable areas for specific OH2 (water) probe.
		Electron density map analysis with Coot	Model analysis -i.e. checking that the atomic model agrees with the experimentally derived electron density.
		B-factors analysis from PDB files	B-factor is an indicator of thermal atom motion, therefore, it allows to evaluate the strength of evidence for their presence.
	- Molecular Interaction Fields (MIF)	GRID analysis with N1, DRY, F probes	It enables the analysis of energetic favorable areas.
ii) Molecular recognition	- Docking	Induced fit Docking protocol implemented into Schrödinger Suite	Exploration of binding modes and the associated conformational changes within receptor active sites.
	- Dynamic simulation	Desmond	It provides insights concerning the internal motions of the complexes by considering it a dynamic model in explicit aqueous solvent.
iii) Energy evaluation	- Mutational free energy perturbation (FEP)	Desmond	FEP calculations for the mutation of a ligand functional group.

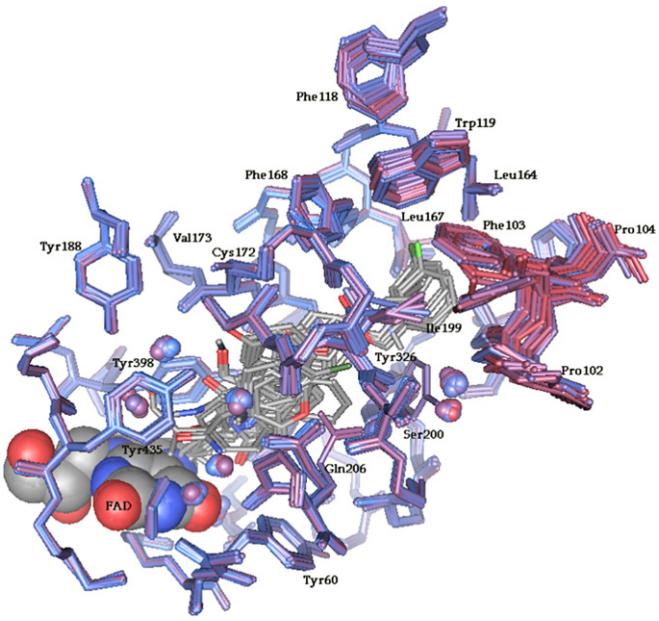

Fig. 1. Alignment of twenty MAO-B PDB complexes. The residues (sticks) and conserved water molecules (spheres) are colored according to b-factor: blue indicates low, violet intermediate and red high temperatures respectively. Ligands co-crystallized (sticks) and FAD cofactor (spacefill) are colored by CPK notation. (For interpretation of the references to colour in this figure legend, the reader is referred to the web version of this article.)

water molecules GRID maps [28] were computed and analyzed. The GRID program calculates favorable interaction sites between a certain target and a selected probe, mimicking a chemical moiety [29]. The approach has been applied successfully for the investigation of water molecules in several studies [30,31]. The water (OH2) probe energies of interaction were calculated with a grid spacing of 0.5 Å (NPLA (Number of PLanes of grid point per Å) = 2). A cut-off value of −8 kcal/mol was chosen to detect, with the combination of MINIM and FILMAP utilities, the most favorable locations for water molecules. Furthermore, the analysis of the water molecules was extended to electron density maps [32] using Coot [33] software and the b-factors reported in PDB structural data (Fig. 2).

3.3. Docking experiments

In order to overcome the limitation of most traditional docking techniques, that consider the protein rigid, we decided to apply the IFD workflow included in the Schrödinger Software Suite [34]. This is a novel method for modeling the conformational changes induced by ligand binding, which uses the combination of the docking program Glide [34], to account for ligand flexibility, and Prime [34], for side-chain rearrangements and minimization of the residues within the binding pocket [35].

First, we docked three reference reversible inhibitors available as co-crystallized structures and then our synthesized compounds. The compounds co-crystallized are two coumarin derivatives **C17** and **C18** available in PDB 2v60 and 2v61 respectively, and the safinamide, **SAG**, a benzyloxy-benzylaminopropionamide in 2v5z [11]. The input structures were built using Maestro and optimized employing Macromodel applying MMFFs (Merck Molecular Force Field). Water was considered implicitly; the PRCG (Polak-Ribier Conjugate Gradient) method was used for minimization, allowing 500 maximum iterations and a 0.05 kcal/(molÅ) convergence threshold. The structures obtained were docked into PDB structure 2v61 after preparation of the enzyme employing the Schrödinger protein preparation wizard [34]. The workflow includes the assignment of correct atom bond orders, the addition of hydrogen, the optimization of hydrogen bonds, the determination of the most favorable ligand protonation state, and the minimization of the protein. Only the water molecules conserved within the binding site were preserved. The IFD workflow consists of a grid setup, followed by three docking steps: Glide rigid docking, Prime induced fit docking, and Glide re-docking. A grid extended to 26 Å around the co-crystallized ligand was defined. The ligands were docked using a scaling factor of 0.5 for the van der Waals radii of both the receptor and the ligands, generating a maximum of 20 poses. The calculated protein–ligand complexes were then refined using Prime: residues within a 5 Å distance range from the ligand were energy minimized using the OPLS 2005 force field. Only the poses showing Prime energies below or equal to 30 kcal/mol, above the lowest conformation energy, were re-docked using the extra precision method (XP) and scored. The XP Score turned out to be the best score for the docked reference inhibitors and, therefore, it was also used to select the poses for the synthesized compounds (see Supplementary data (SD) Table S1, S2).

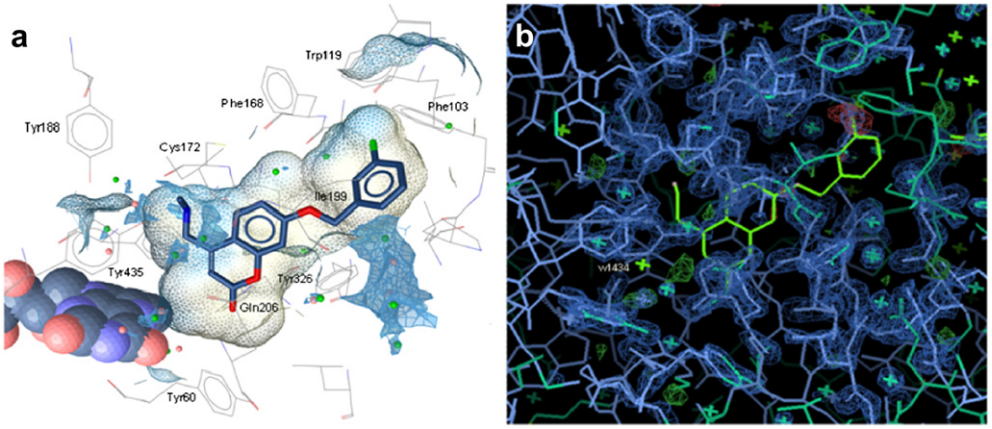

Fig. 2. Water analysis. a) LigandScout visualization of the water probe GRID maps calculated from PDB entry 2v61 (dark blue) in which **C18** 7-[(3-chlorophenyl)methoxy]-4-(methylaminomethyl)chromen-2-one is co-crystallized with hMAO-B. Minimum points of the GRID maps are illustrated as green spheres; conserved co-crystallized water molecules in the binding site are indicated as red spheres, ligand as sticks, and the cofactor in space fill representation. The receptor binding pocket is visualized as a wireframe model colored according to lipophilicity: light blue for hydrophilic and pale yellow for hydrophobic residues. b) Electron density map of PDB complex 2v61 visualized in Coot, with the 2*Fo*−*Fc* map (blue), the positive density of the *Fo*−*Fc* map (i.e., parts of the electron density not represented in the model, in green), and the negative density (i.e., parts of the model that are not backed up by electron density, in red). Protein, ligand, and water are colored by b-factor: From dark blue for low b-factor to cyan and green for higher b-factor. (For interpretation of the references to colour in this figure legend, the reader is referred to the web version of this article.)

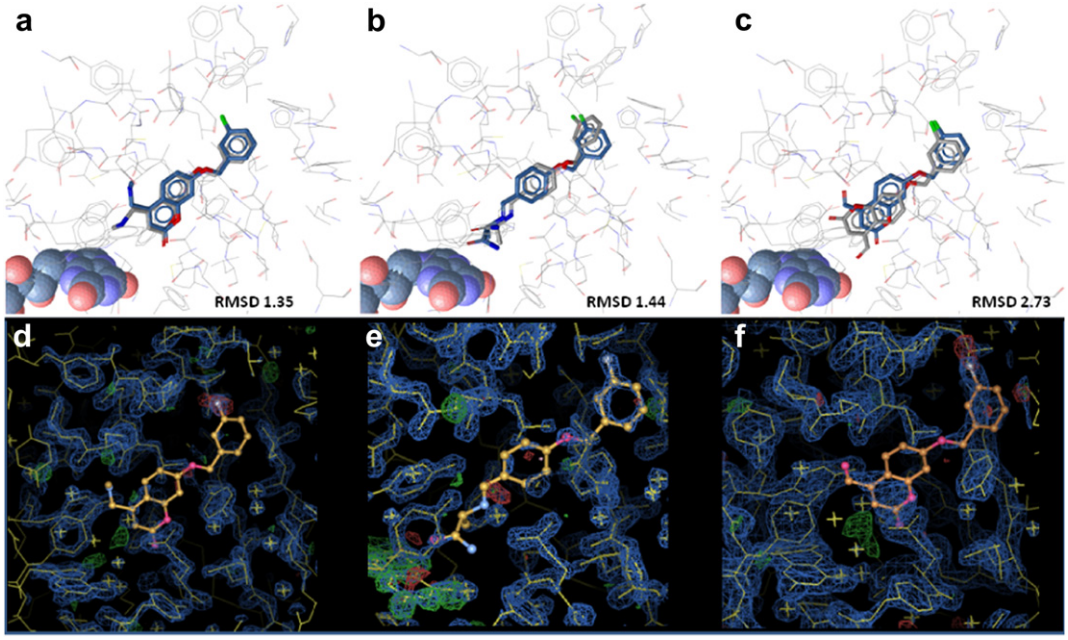

Fig. 3. Comparison of the crystallized (in blue) and docked poses (in gray) of ligands. a) **C18**-7-[(3-chlorophenyl)methoxy]-4-(methylaminomethyl)chromen-2-one, b) **SAG**-(*S*)-(+)-2-[4-(fluorobenzyloxy-benzylamino)propionamide] and c) **C17**-7-[(3-chlorophenyl)methoxy]-2-oxo-chromene-4-carbaldehyde docked into the MAO 2v61 PDB model, with the FAD displayed as CPK colored space fill rendering and the closest residues as wireframe. The electron density maps of the original complex are reported in d) **C18**-2v61, e) **SAG**-2v5z and f) **C17**-2v60 panels. (For interpretation of the references to colour in this figure legend, the reader is referred to the web version of this article.)

3.3.1. Docking of reference compounds

The IFD workflow reproduced the binding mode of three co-crystallized compounds with an RMSD (Root-Mean-Square Deviation) ranging from 1.3 to 2.7 Å (Fig. 3, SD Table S1).

It is always the object of scientific discussion whether the root-mean-square distance (RMSD) calculation is valid for docking performance evaluation and several papers address the drawbacks of RMSD, suggesting other approaches for the evaluation of predicted and experimental pose, like IBAC (Interactions-Based Accuracy Classification) [36] and RSR (Real Space R-factor) [37]. This latter descriptor takes the electron density maps into account. In our case, the pose of **C18**-2v61 (Fig. 3a) was well predicted except for the methylamino substituent, however, the electron density maps of this particular area raise doubts about the exclusive location of the methylamino substituent as proposed by the X-ray structural model. (Fig. 3d) These observations indicate the docked orientation of this portion also as plausible. The co-crystallized compound **C17**, reported in 2v60 PDB complex (Fig. 3c,f), is predicted with the lowest accuracy considering the RMSD. Also in this case, the portion not well predicted (i.e., the coumarin moiety) has no directional interaction (i.e. hydrogen bonds) with the protein and, by considering the electron density maps, we judged this docking pose as acceptable too. Finally, **SAG**-2v5z was docked correctly and showed RMSD equal to 1.44 Å (Fig. 3b,e).

3.3.2. Docking of synthesized compounds

The input structures were built using Maestro as described above. The *E*-configuration of these compounds is known to be energetically favorable – as also confirmed by a previous computational study performed on a similar molecule [7]. Therefore, the *E*-configuration was used for the docking experiments. Visual inspection of the docking results highlighted many of the compounds double binding on the best-scored poses. The two configurations resulted rotated 180°: with the halogen atom close to the entrance cavity toward the external part of the enzyme (binding mode **I**) or in the catalytic cavity pointing toward the cofactor (binding mode **II**). Coexistence of multiple binding modes has to be taken into consideration after docking experiments [38]. As the aim of this work is to gain some insight into the binding mode in order to optimize activity by keeping the great selectivity for the MAO-B isoform, we decided to follow up the docking study with a molecular dynamics simulation on the complex of **5a**, the best compounds of the **a** series, and **5b**, the analog compound where F was replaced with Cl. The poses with the lowest XP Score of the two different binding modes of both compounds (SD Table S2) were submitted to MD simulation by Desmond.

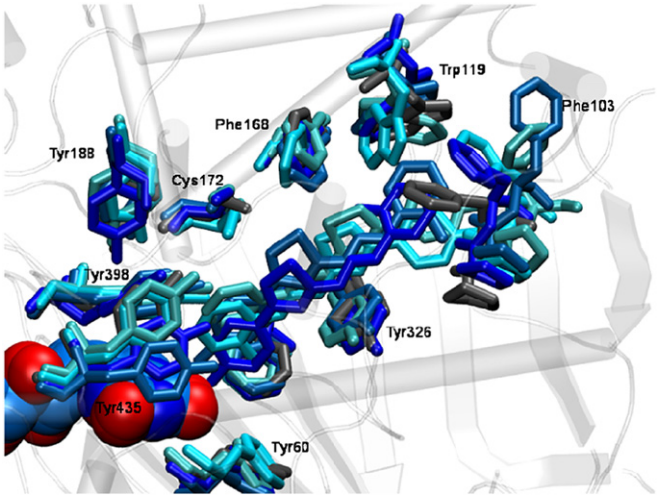

Fig. 4. Superimposition of average MD poses of **5a-I** (cyan), **5a-II** (dark blue), **5b-I** (light blue), **5b-II** (marine) onto the crystallographic model 2v61 (gray) showing the flexibility of some residues of Phe99-Tyr112 loop. (For interpretation of the references to colour in this figure legend, the reader is referred to the web version of this article.)

Table 3
Relative binding, solvation and difference free energies in kcal/mol in the FEP analysis.

Compound	Mutation	ΔG-complex	ΔG-solvent	ΔΔG
5a-I	F → Cl	0.75 ± 0.12	0.55 ± 0.08	0.21
5a-II	F → Cl	3.40 ± 0.15	0.68 ± 0.09	2.72

3.4. Molecular dynamic simulations and free energy perturbation analysis

The complexes were solvated with a 10 Å box of TIP3P (Transferable Intermolecular Potential 3-Point) water [39] and counter ions were added to neutralize the system net charge. The solvated models were relaxed and energy minimized, and subsequently the MTK_NPT (Martyna-Tobias-Klein with constant Number of particles, Pressure and Temperature) ensemble was employed. The default stages in the relaxation process for the NPT ensemble include two energy minimizations, and four simulation steps. During the energy minimizations, two runs of 2000 iteration steps were processed using the steepest descent method: during the first run, the protein structure was fixed by a force restraint constant of 50 kcal/(molÅ) and in the second all restraints were released. With the first simulation, at NVT (constant Number of particles, Volume, and Temperature) ensemble, the system reached a temperature of 10 K. In the following three simulations in the NPT ensemble, the system was heated up to 300 K and the pressure was kept constant at 1 bar using the Berendsen thermostat–barostat. During the production phase, temperature and pressure were kept constant using the Nosè-Hoover thermostat–barostat. The energy and trajectory were recorded every 1.2 ps and 4.8 ps, respectively. For multiple time step integration, RESPA (REversible reference System Propagator Algorithm) [40] was applied to integrate the equation of motion with Fourier-space electrostatics computed every 6 fs, and all remaining interactions computed every 2 fs. All chemical bond lengths involving hydrogen atoms were fixed with SHAKE [41]. Short range cut-off was set to 9 Å and the smooth particle mesh Ewald method (PME) [42] was used for long range electrostatic interaction. The analysis of the trajectories were performed with Desmond simulation analysis event and VMD [43]. Finally, the average structure of the last ns of the simulation of both binding modes, named **I** and **II**, was energy minimized and used as a starting point to run FEP analysis by Desmond software [44], in order to estimate the free energy variation as functional of F *vs* Cl.

4. Results and discussion

Tested compounds (novel compounds as well as and reference inhibitors) themselves were unable to react directly with the Amplex Red reagent, demonstrating no interference with the measurements. In our experiments, hMAO-A displayed a Michaelis constant (K_m) of 514 ± 46.8 μM and a maximum reaction velocity (V_{max}) of 301.4 ± 27.9 nmol/min/mg protein, whereas hMAO-B showed a K_m of 104.7 ± 16.3 μM and a V_{max} of 28.9 ± 6.3 nmol/min/mg protein ($n = 5$). All synthesized compounds were inactive toward MAO-A below 100 μM, suggesting the 1-aryliden-2-(4-(4-halophenyl)thiazol-2-yl)hydrazine as a promising candidate scaffold for the design of selective MAO-B inhibitors. Moreover, compounds (**1**–**6**)**b**, bearing a chlorine atom in the *para* position of the phenyl moiety, turned out to be inactive toward the B isoform. However, compounds (**1**–**6**)**a**, were all active in the nM–μM range (Table 1). The substitution at the phenyl moiety in position two of thiazole showed to modulate the activity within the **a** series. In particular, in cases where no substitution (**1a**) or a 2-methyl group was introduced in this ring (**2a**), the compounds exhibited activity in the nanomolar range, while substitution in other phenyl positions with chlorine, methyl or methoxy group led to an activity decrease. Minor changes in this scaffold result in wide changes in activity.

Firstly, we analyzed the alignment of twenty available complexes. The result of the structure comparison is shown in Fig. 1: the substrate cavity is quite rigid; no remarkable shift in the alpha carbon (Cα) position was observed, in accordance to previously reported findings [45]. However, it needs to be pointed out, that a few residues within the substrate cavity (i.e., Gln206, Cys172,

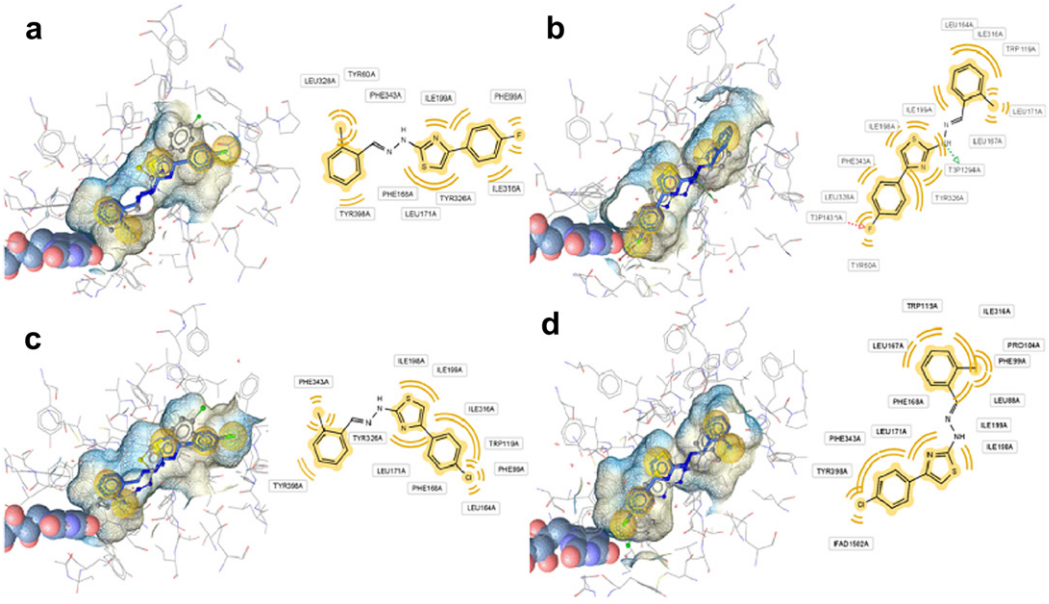

Fig. 5. Average conformations of MD trajectories. Compounds are represented in sticks, starting geometries in ball and sticks, FAD in space fill models, respectively. Pharmacophoric features are visualized as green (HB-donor), red (HB-acceptor) arrows, and yellow spheres (hydrophobic interactions). The surface of the binding pocket is represented in wireframe, colored in accordance to lipophilicity: pale yellow indicates lipophilic and light blue hydrophilic residues. Binding modes and 2D depictions of interactions are reported for **5a-I**, **5a-II**, **5b-I** and **5b-II** respectively in panels a), b), c) and d). (For interpretation of the references to colour in this figure legend, the reader is referred to the web version of this article.)

Leu171, and Phe343) were characterized by side chain conformational flexibility among the different crystal structures (SD Table S3a). The shift of these chains could influence the interactions between enzyme and inhibitors. Moreover, the higher b-factors (Fig. 1) and Cα-RMSD values (SD Table S3b) of residues forming the entrance cavity clearly indicate this portion of the enzyme is rather flexible. In previous studies, the role of Ile199 as a gatekeeper between both cavities was published. Rotation of the Ile199 side chain allows for fusion of the two cavities and could be observed upon binding of inhibitors across both cavities [46]. In addition, an important role of the Phe99-Tyr112 loop in regulating substrate recognition has been reported [47,48]. Hence, induced fit docking experiments appear to be a suitable approach for reproducing experimental observations.

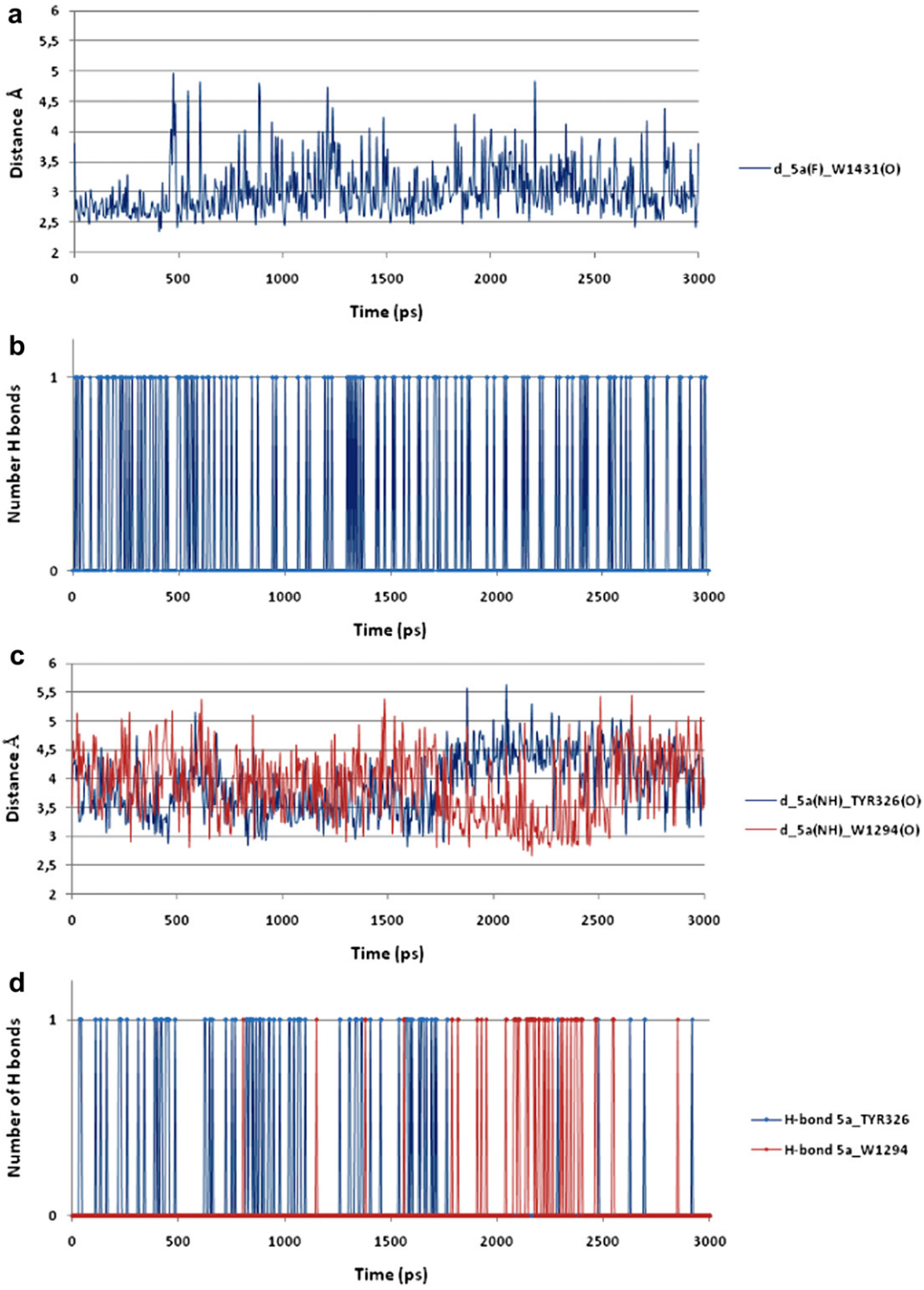

Fig. 6. MD trajectory analysis. a) Distances between F in **5a-II** and O-W1431; b) number of hydrogen bonds between F and W1431; c) distance of NH-**5a-II** from O-Tyr326 and O-W1294; d) number of hydrogen bonds between **5a-II**-Tyr326 and **5a-II** W1294.

Water molecules located within the binding pocket (W1122, W1207, W1220, W1221, W1294, W1295, W1387, W1388, W1431; numbering according to 2v61) were preserved. Besides the fact that these water molecules are conserved in several crystal structures (Fig. 1) and show multiple interactions with the protein, a correspondence with the most favorable water positions obtained from GRID was observed: energy minimum points for water probe of the GRID-molecular interaction fields were close to the position of waters observed in the crystal structure (Fig. 2a). Furthermore, the analysis of the electron density maps demonstrated all nine water molecules are well defined and characterized by a low b-factor (i.e., b-factor range is between 9 and 16) (Fig. 2b). In the 2v61 model water molecule (W1434) was not considered since it was missing in the majority of crystal structures. Moreover, it was characterized by a b-factor value of 23, rather high if compared to the surrounding waters and residues; also, its corresponding electron density map resulted quite poor at this point (Fig. 2b).

In order to describe realistically protein–ligand interactions, it is necessary to take into account the structural modification in both the receptor and the ligand during the host/guest recognition. However, in classic docking approaches, the receptor is usually treated as being rigid or semi-rigid. The analysis of the alignment, as discussed above, indicated the entrance cavity of the enzyme as rather flexible and this aspect may be important in the recognition of bulky compounds. Using the IF approach, the side chains near the inhibitor were kept flexible. The XP Score was not able to explain the huge difference in activity of the two series of compounds (SD Table S1). Looking at the best-scored poses, it appeared clear that two main binding modes are possible. We decided to focus our attention on the best compound **5a** and the correspondent chloro-substituted **5b**. Both binding modes were analyzed. In the binding mode **I** the phenyl substituent in four position of the thiazole is orientated toward the entrance cavity, conversely in the **II** toward the FAD cofactor. Then we ran a 3 ns MD simulation for each molecule except for the **5b**-**II** where, due to increasing RMSD, and we decided to extend the simulation up to 5 ns (Fig. S4, SD).

The resulting poses of IFD were thereby taken as a starting structure for the MD simulations. All four complexes resulted as being stable. As shown in Fig. 3, the residues in the catalytic cavity are rather rigid, while residues in the entrance cavity (Phe103 and Trp119 in particular) moved slightly in order to better accommodate the compounds. The average structure of each complex was energy minimized and analyzed (Fig. 4).

Furthermore, to obtain more information about a preferential binding mode and to corroborate the experimental data, we have performed FEP simulations focusing our attention on the effect of group mutation: fluorine with chlorine. Table 3 shows the estimation of free energy variation ($\Delta\Delta G$) for such substituent change. Confirming the experimental data, the FEP analysis demonstrates that the substitution is unfavorable. Moreover, only the energetic difference of the second pose is able to explain the large difference in terms of activity. From this analysis, we assume that the binding mode proposed by the second pose is the most favorable.

The ability of the compound **5a** to be placed across both cavities illustrates the reason why these compounds are selective for MAO-B. The arylidene portion is accommodated within the cavity access of the enzyme and is stabilized by hydrophobic interactions with Trp119, Leu164, Leu167, Leu171, Ile316. Pharmacophoric interactions are visualized using LigandScout [49]. The analysis of the interactions stabilizing the complex highlighted a key role of the water molecules complex stabilization: during the whole MD simulation the fluorine atom interacts with W1431 molecule (Figs. 5b and 6a,b). In the crystal structure this structural water is involved in HB with FAD and Lys296. After docking and during the MD it bridges the compound **5a** to Gly58 and Lys296. In the last part of the dynamic simulation (Fig. 6c,d) a second molecule, W1294, in the crystal structure interested in HB contacts respectively with Gln206, Thr201 and Ile199, is also implicated in bridging the compound **5a** to the protein (Tyr326).

The visual inspection of the binding mode of the compound **5a** suggested that substitution with bulky groups in positions 3 and 4 of the phenyl ring should prevent a good fit in this pocket causing the loss of complex interactions mentioned above. This observation provides a rational explanation for the decreased activity of some of the compounds of the **a** series. This is even more evident in the case of compound **5b**, which is kept more distant from the cofactor and, to accommodate it, the Phe103 has to assume an open conformation. The simple substitution of the F with Cl does not allow the

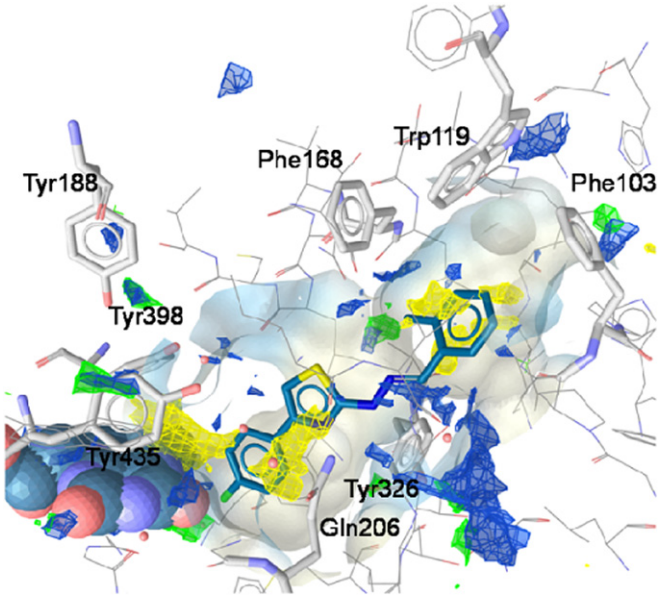

Fig. 7. GRID maps and **5a**-**II** binding mode: yellow DRY probe, blue N1 probe, green F probe. (For interpretation of the references to colour in this figure legend, the reader is referred to the web version of this article.)

compound to be stabilized by any hydrogen bond, but only by hydrophobic interactions (Fig. 5d). To further support the **II** binding mode of **5a** we calculated the GRID maps with the DRY probe, for detection of favorable hydrophobic areas; N1, to locate favorable areas for amino groups and Fluorine (F) probe. The analysis and visualization of these maps confirmed our hypothesis of binding mode (Fig. 7). Therefore a reason of **a** series better activity could be the presence of a less bulky and more electronegative group (F *vs* Cl) which allows a better accommodation in the binding pocket and make possible the stabilization of the complex with H bond.

Additionally we also investigated the ADME profile of the compound with Qikprop [34] summarized in Table S5 of SD. The prediction indicates that the compound has good drug-like characteristics: good oral absorption, does not show any violation of Lipinski's [50] and Jorgesen's [51] rules, good activity for central nervous system which allowed us to be more confident that such compound would target the area directly involved in the etiology of neurodegenerative disorders.

5. Conclusions

We have synthesized and investigated the biological activity of two closely related series of compounds that show a high gap inhibition activity. In order to understand the possible binding mode and to rationalize the activity, we have performed several computational investigations. Due to the flexibility of the entrance cavity, we have carried out IFD experiment, followed by MD simulations and FEP calculations. The modeling methods employed allowed us to derive structure–activity relationships that highlighted the importance of the presence of a fluorine substituent interacting with the water close to the cofactor as well as the importance of substituent position in the arylidene moiety. The key interactions can then be used to derive conclusions and will be taken into account for further modifications on this promising scaffold which showed great selectivity for the MAO-B isoform. Moreover, relevant pharmacophoric features have been resolved and will constitute the basis for future work.

6. Experimental section

6.1. Chemistry

6.1.1. General methods

Melting points were uncorrected and were determined on a Reichert Kofler thermopan apparatus. TLC analyses were performed on silica gel 60 F254 plates; spots were visualized by UV light. All synthesized compounds were purified by crystallization from an appropriate solvent (ethanol, ethanol/2-propanol). Elemental analyses were obtained on a Perkin Elmer 240 B microanalyzer. Electron ionization (EI) mass spectra were obtained by a Fisons QMD 1000 mass spectrometer (70 eV, 200 μA, ion source temperature 200 °C). The samples were introduced directly into the ion source. High resolution mass spectra (HRMS) were recorded using a QSTAR XL hybrid quadrupole time-of-flight mass spectrometer from AB Sciex (Foster City, CA). Analytes were solubilized in methanol at a concentration of 0.5 mg/mL and subsequently diluted in infusion solvent (acetonitrile:formic acid:water 50/0.1/19.9 v/v) at a concentration of 5 μg/mL. Analyte solutions were infused at 5 μL/min into the mass spectrometer operating in positive ion mode.

^{1}H NMR spectra were recorded on a Varian (300 MHz) or on a Varian Unity 600 (600 MHz); deuterated DMSO was used as solvents. Chemical shifts are expressed as δ units (parts per million) using TMS as an internal standard. Coupling constants J are valued in Hertz (Hz).

6.1.2. General procedure

For the preparation of compounds **1**–**6**. In a two-necked flask a mixture of arylidenethiosemicarbazide (0.0051 mol), and 2-halogenacetophenone (0.0061 mol) are refluxed, under vigorous stirring in 20 ml of 2-propanol. The reaction is refluxed for a period ranging between 30 and 120′, until completion by TLC (ethyl acetate/hexane). The formation of a foaming product, which precipitates, is observed upon cooling down to room temperature. The solid precipitate is filtered and crystallized from ethanol or ethanol/2-propanol. Elemental analyses were within ±0.4% of the theoretical values. All compounds exhibit well-detectable molecular ions in EI conditions. HRMS full scan and MS/MS are available as SD.

6.1.3. Analysis

*6.1.3.1. 1-Benzylidene-2-[4-(4-fluorophenyl)thiazol-2-yl]hydrazine (**1a**).* Pale yellow solid, yield 82%; mp 189–191 °C; ^{1}H NMR (300 MHz, DMSO-d_6) δ = 7.37 (t, 2H, $H_{aromatics}$, J = 8.4); 7.44 (s, 1H, C_5H-thiaz.); 7.51–7.59 (m, 3H, $H_{aromatics}$); 7.79 (d, 2H, $H_{aromatics}$, J = 7.7); 8.02 (dd, 2H, $H_{aromatics}$, J = 7.3, 5.4); 8.19 (s, 1H, CH═N); 9.25 (s, 1H, NH, D_2O-exch.).

*6.1.3.2. 1-(4-Chlorobenzylidene)-2-[4-(4-fluorophenyl)thiazol-2-yl] hydrazine (**2a**).* Pale yellow solid, yield 74%; mp 195–197 °C; ^{1}H NMR (300 MHz, DMSO-d_6) δ = 7.24 (t, 2H, $H_{aromatics}$, J = 8.8); 7.33 (s, 1H, C_5H-thiaz.); 7.49 (d, 2H, $H_{aromatics}$, J = 8.4); 7.68 (d, 2H, $H_{aromatics}$, J = 8.4); 7.89 (dd, 2H, $H_{aromatics}$, J = 8.3, 5.8); 8.04 (s, 1H, CH═N); 12.33 (s, 1H, NH, D_2O-exch.).

*6.1.3.3. 1-(3,4-Dimethoxybenzylidene)-2-[4-(4-fluorophenyl)thiazol-2-yl]hydrazine (**3a**).* Pale pink powder, yield 95%; mp 194–196 °C; ^{1}H NMR (400 MHz, DMSO-d_6) δ = 3.95 (s, 6H, OCH_3); 6.70 (s, 1H, C_5H-thiaz.); 6.92 (d, 1H, $H_{aromatics}$, J = 8.4); 7.7.16–7.22 (m, 3H, $H_{aromatics}$) 7.29 (d, 1H, $H_{aromatics}$, J = 2.0); 7.73 (dd, 2H, $H_{aromatics}$, J = 8.5, 5.0); 8.16 (s, 1H, CH═N); 9.01 (s, 1H, NH, D_2O-exch.).

*6.1.3.4. 1-(4-Methoxybenzylidene)-2-[4-(4-fluorophenyl)thiazol-2-yl]hydrazine (**4a**).* Yellow powder, yield 94%; mp 198–200 °C; ^{1}H NMR (300 MHz, DMSO-d_6) δ = 3.79 (s, 3H, OCH_3); 7.00 (d, 2H, $H_{aromatics}$, J = 8.6); 7.23 (t, 2H, $H_{aromatics}$, J = 8.8); 7.28 (s, 1H, C_5H-thiaz.); 7.60 (d, 2H, $H_{aromatics}$, J = 8.6); 7.88 (dd, 2H, $H_{aromatics}$, J = 8.2, 5.9); 8.02 (s, 1H, CH═N); 9.65 (s, 1H, NH, D_2O-exch.).

*6.1.3.5. 1-(2-Methylbenzylidene)-2-[4-(4-fluorophenyl)thiazol-2-yl] hydrazine (**5a**).* Brilliant yellow powder, yield 100%; mp 195–198 °C; ^{1}H NMR (400 MHz, DMSO-d_6) δ = 2.56 (s, 3H, CH_3); 7.33–7.40 (m, 6H, $H_{aromatics}$ + C_5H-thiaz.); 7.82–7.85 (m, 1H, $H_{aromatics}$); 8.02 (dd, 2H, $H_{aromatics}$, J = 7.3, 5.4); 8.47 (s, 1H, CH═N); 9.17 (s, 1H, NH, D_2O-exch.).

*6.1.3.6. 1-(4-Methylbenzylidene)-2-[4-(4-fluorophenyl)thiazol-2-yl] hydrazine (**6a**).* Pale yellow powder, yield 92%; mp 194–195 °C; ^{1}H NMR (300 MHz, DMSO-d_6) δ = 2.46 (s, 3H, CH_3); 7.34–7.42 (m, 5H, $H_{aromatics}$ + C_5H-thiaz.); 7.67 (d, 2H, $H_{aromatics}$, J = 6.4); 8.02 (dd, 2H, $H_{aromatics}$, J = 7.3, 5.4), 8.14 (s, 1H, CH═N) 9.65 (s, 1H, NH, D_2O-exch.).

*6.1.3.7. 1-Benzylidene-2-[4-(4-chlorophenyl)thiazol-2-yl]hydrazine (**1b**).* White powder, yield 89%; mp 222–224 °C; ^{1}H NMR (300 MHz, DMSO-d_6) δ = 7.38–7.48 (m, 6H, $H_{aromatics}$ + C_5H-thiaz.); 7.66 (d, 2H, $H_{aromatics}$, J = 7.9); 7.87 (d, 2H, $H_{aromatics}$, J = 8.5); 8.05 (s, 1H, CH═N); 8.75 (s, 1H, NH, D_2O-exch.).

*6.1.3.8. 1-4-Chlorobenzylidene-2-[4-(4-chlorophenyl)thiazol-2-yl] hydrazine (**2b**).* Brown powder, yield 100%; mp 215–217 °C; ^{1}H NMR (300 MHz, DMSO-d_6) δ = 7.53 (s, 1H, C_5H-thiaz.); 7.57–7.63

(m, 4H, $H_{aromatics}$); 7.80 (d, 2H, $H_{aromatics}$, $J = 8.4$); 7.99 (d, 2H, $H_{aromatics}$, $J = 8.4$); 8.44 (s, 1H, CH=N); 12.36 (s, 1H, NH, D_2O-exch.).

*6.1.3.9. 1-(3,4-Dimethoxybenzylidene)-2-[4-(4-chlorophenyl)thiazol-2-yl]hydrazine (**3b**).* Pale pink powder, yield 90%; mp 214–216 °C; ^1H NMR (300 MHz, DMSO-d_6) $\delta = 3.79$ (s, 3H, OCH_3); 3.81 (s, 3H, OCH_3); 7.01 (d, 1H, $H_{aromatics}$, $J = 8.3$); 7.17 (d, 1H, $H_{aromatics}$, $J = 8.3$); 7.26 (s, 1H, $H_{aromatics}$); 7.37 (s, 1H, C_5H-thiaz.); 7.46 (d, 2H, $H_{aromatics}$, $J = 8.3$); 7.86 (d, 2H, $H_{aromatics}$, $J = 8.3$); 7.97 (s, 1H, CH=N); 8.98 (s, 1H, NH, D_2O-exch.).

*6.1.3.10. 1-(4-Methoxybenzylidene)-2-[4-(4-chlorophenyl)thiazol-2-yl]hydrazine (**4b**).* Yellow solid, yield 92%; mp 232–235 °C; ^1H NMR (300 MHz, DMSO-d_6) $\delta = 3.79$ (s, 3H, OCH_3); 7.00 (d, 2H, $H_{aromatics}$, $J = 8.5$); 7.37 (s, 1H, C_5H-thiaz.); 7.46 (d, 2H, $H_{aromatics}$, $J = 8.3$); 7.60 (d, 2H, $H_{aromatics}$, $J = 8.5$); 7.86 (d, 2H, $H_{aromatics}$, $J = 8.3$), 8.02 (s, 1H, CH=N); 10.29 (s, 1H, NH, D_2O-exch.).

*6.1.3.11. 1-(2-Methylbenzylidene)-2-[4-(4-chlorophenyl)thiazol-2-yl] hydrazine (**5b**).* Red powder, yield 94%; mp 210–212 °C; ^1H NMR (300 MHz, DMSO-d_6) $\delta = 2.56$ (s, 3H, CH_3); 7.37–7.41 (m, 3H, $H_{aromatics}$); 7.51 (s, 1H, C_5H-thiaz.); 7.58 (d, 2H, $H_{aromatics}$, $J = 8.4$); 7.82 (t, 1H, $H_{aromatics}$, $J = 7.7$); 7.99 (d, 2H, $H_{aromatics}$, $J = 8.5$), 8.41 (s, 1H, CH=N); 8.86 (s, 1H, NH, D_2O-exch.).

*6.1.3.12. 1-(4-Methylbenzylidene)-2-[4-(4-chlorophenyl)thiazol-2-yl] hydrazine (**6b**).* Pale yellow powder, yield 96%; mp 224–226 °C; ^1H NMR (300 MHz, DMSO-d_6) $\delta = 2.46$ (s, 3H, CH_3); 7.37–7.39 (m, 3H, $H_{aromatics}$, and C_5H-thiaz.); 7.52 (s, 1H, NH, D_2O-exch.); 7.59 (d, 2H, $H_{aromatics}$, $J = 7.7$); 7.68 (d, 2H, $H_{aromatics}$, $J = 7.7$); 8.00 (d, 2H, $H_{aromatics}$, $J = 7.3$), 8.14 (s, 1H, CH=N); 9.84 (s, 1H, NH, D_2O-exch.).

6.2. Biochemistry studies

6.2.1. Determination of hMAO isoform activity

The potential effects of the tested compounds on hMAO activity were investigated by measuring their effects on the production of hydrogen peroxide from *p*-tyramine (a common substrate for both hMAO-A and hMAO-B), using the Amplex® Red MAO assay kit (Molecular Probes, Inc., Eugene, Oregon, USA) and microsomal MAO isoforms prepared from insect cells (BTI-TN-5B1-4) infected with recombinant baculovirus containing cDNA inserts for hMAO-A or hMAO-B (Sigma–Aldrich Química S.A., Alcobendas, Spain).

The production of H_2O_2 catalyzed by MAO isoforms can be detected using 10-acetyl-3,7-dihydroxyphenoxazine (Amplex® Red reagent), a non-fluorescent and highly sensitive probe that reacts with H_2O_2 in the presence of horseradish peroxidase to produce the fluorescent product resorufin. In this study hMAO activity was evaluated using the above fluorimetric method following the general procedure described previously by us [19,52].

0.1 mL of sodium phosphate buffer (0.05 M, pH 7.4) containing the test drugs (new compounds or reference inhibitors) in various concentrations and adequate amounts of recombinant hMAO-A or hMAO-B required and adjusted to obtain the same reaction velocity in our experimental conditions, i.e., to oxidize (in the control group) 165 pmol of *p*-tyramine/min (hMAO-A: 1.1 μg protein; specific activity: 150 nmol of *p*-tyramine oxidized to *p*-hydroxyphenylacetaldehyde/min/mg protein; hMAO-B: 7.5 μg protein; specific activity: 22 nmol of *p*-tyramine transformed/min/mg protein), were incubated for 15 min at 37 °C in a flat-black-bottom 96-well microtest™ plate (BD Biosciences, Franklin Lakes, NJ, USA) placed in a dark fluorimeter chamber. After this incubation period, the reaction was started by adding (final concentrations) 200 μM Amplex® Red reagent, 1 U/mL horseradish peroxidase and 1 mM *p*-tyramine. The production of H_2O_2 and, consequently, of resorufin was quantified at 37 °C in a multidetection microplate fluorescence reader (FLX800TM, Bio-Tek® Instruments, Inc., Winooski, VT, USA) based on the fluorescence generated (excitation, 545 nm, emission, 590 nm) over a 15 min period, in which the fluorescence increased linearly.

Control experiments were carried out simultaneously by replacing the test drugs (new compounds and reference inhibitors) with appropriate dilutions of the vehicles. In addition, the potential ability of the test drugs to modify the fluorescence generated in the reaction mixture due to non-enzymatic inhibition (e.g., for directly reacting with Amplex® Red reagent) was determined by adding these drugs to solutions containing only the Amplex® Red reagent in a sodium phosphate buffer.

To determine the kinetic parameters of hMAO-A and hMAO-B (K_m and V_{max}), the corresponding enzymatic activity of both isoforms was evaluated (under the experimental conditions described above) in presence of a number (a wide range) of *p*-tyramine concentrations.

The specific fluorescence emission (used to obtain the final results) was calculated after subtraction of the background activity, which was determined from vials containing all components except the hMAO isoforms, which were replaced by a sodium phosphate buffer solution.

6.2.2. Data presentation and statistical analysis

Unless specified otherwise, the results shown in the text and tables are expressed as mean ± standard error of the mean (S.E.M.) from *n* experiments. Significant differences between two means ($P < 0.01$) were determined by one-way analysis of variance (ANOVA) followed by the Dunnett's *post-hoc* test.

To study the possible effects of the test drugs (new compounds or reference inhibitors) on MAO isoform enzymatic activity, we evaluated the variation of fluorescence per unit of time (fluorescence arbitrary U/min) and, indirectly, the rate of hydrogen peroxide (H_2O_2) production, and therefore the pmol/min of resorufin produced in the reaction between H_2O_2 and Amplex® Red reagent. For this purpose, several concentrations of resorufin were used to prepare a standard curve with X = pmol resorufin and Y = fluorescence arbitrary U. Note that the value of resorufin production is similar to the pmol of *p*-tyramine oxidized to *p*-hydroxyphenylacetaldehyde/min, since the stoichiometry of the reaction (*p*-tyramine oxidized by MAO isoforms/resorufin produced) is 1:1.

In these experiments, the inhibitory activity of the tested drugs (new compounds and reference inhibitors) is expressed as IC_{50}, i.e., the concentration of these compounds required for a 50% reduction of the control MAO isoform enzymatic activity, estimated by least-squares linear regression, using the Origin™ 5.0 program (Microcal Software, Inc., Northampton, MA, USA), with X = log of tested compound molar concentration and Y = the corresponding percentage of inhibition of control resorufin production obtained with each concentration. This regression was performed using data obtained with 4–6 different concentrations of each tested compound which inhibited the control MAO isoform enzymatic activity by between 20 and 80%. Kinetic parameters (K_m and V_{max}) of hMAO-A and hMAO-B were estimated using the GraphPad Prism 5.0 software (GraphPad Software Inc., San Diego, CA, USA).

6.2.3. Drugs and chemicals

The drugs, vehicle and chemicals used in the experiments were the new compounds, moclobemide (a generous gift from F. Hoffmann-La Roche Ltd., Basel, Switzerland), dimethyl sulfoxide (DMSO), *R*-(−)-deprenyl hydrochloride, iproniazid phosphate (purchased from Sigma–Aldrich, Spain), resorufin sodium salt, clorgyline hydrochloride, *p*-tyramine hydrochloride, sodium

phosphate and horseradish peroxidase (supplied in the Amplex® Red MAO assay kit from Molecular Probes).

Appropriate dilutions of the above drugs were prepared every day immediately before use in deionized water from the following concentrated stock solutions kept at −20 °C: the new compounds (0.1 M) in DMSO; *R*-(−)-deprenyl, moclobemide, iproniazid, resorufin, clorgyline, *p*-tyramine and horseradish peroxidase (0.1 M) in deionized water.

Due to the photosensitivity of some chemicals (e.g., Amplex® Red reagent), all experiments were performed in the dark. In all assays, neither deionized water (Milli-Q®, Millipore Ibérica S.A., Madrid, Spain) nor appropriate dilutions of the vehicle used (DMSO) had significant pharmacological effects.

Acknowledgments

The work was supported by Fondazione Banco di Sardegna-Sassari-Italy, Ministerio de Sanidad y Consumo (Spain; FISS PI061537) and Consellería de Innovación e Industria de la Xunta de Galicia (Spain; INCITE07PXI203039ES, INCITE08E1R203054ES and 08CSA019203PR). The authors wish to thank Mr Roberto Maxia for the technical support.

Appendix. Supplementary data

Supplementary data related to this article can be found online at doi:10.1016/j.ejmech.2011.12.027.

References

[1] M.B.H. Youdim, D. Edmondson, K.F. Tipton, The therapeutic potential of monoamine oxidase inhibitors, Nat. Rev. Neurosci. 7 (2006) 295–309.
[2] L.W. Elmer, J.M. Bertoni, The increasing role of monoamine oxidase type B inhibitors in Parkinson's disease therapy, Expert Opin. Pharmacother. 9 (2008) 2759–2772.
[3] J. Saura, J.M. Luque, A.M. Cesura, M. Da Prada, V. Chan-Palay, G. Huber, J. Loffler, J.G. Richards, Increased monoamine oxidase B activity in plaque-associated astrocytes of Alzheimer brains revealed by quantitative enzyme radioautography, Neuroscience 62 (1994) 15–30.
[4] M.J. Kumar, D.G. Nicholls, J.K. Andersen, Oxidative α-ketoglutarate dehydrogenase inhibition via Subtle Elevations in monoamine oxidase B levels results in loss of spare respiratory capacity: implication for Parkinson's disease, J. Biol. Chem. 278 (2003) 46432–46439.
[5] J.J. Chen, D.M. Swope, K. Dashtipour, Comprehensive review of rasagiline, a second-generation monoamine oxidase inhibitor, for the treatment of Parkinson's Disease, Clin. Ther. 29 (2007) 1825–1849.
[6] R.G. Fariello, Safinamide, Neurotherapeutics 4 (2007) 110–116.
[7] F. Chimenti, E. Maccioni, D. Secci, A. Bolasco, P. Chimenti, A. Granese, O. Befani, P. Turini, S. Alcaro, F. Ortuso, M.C. Cardia, S. Distinto, Selective inhibitory activity against MAO and molecular modeling studies of 2-thiazolylhydrazone derivatives, J. Med. Chem. 50 (2007) 707–712.
[8] W.K. Hagmann, The many roles for fluorine in medicinal chemistry, J. Med. Chem. 51 (2008) 4359–4369.
[9] K.L. Kirk, Fluorine in medicinal chemistry: recent therapeutic applications of fluorinated small molecules, J. Fluorine Chem. 127 (2006) 1013–1029.
[10] D.E. Edmondson, C. Binda, J. Wang, A.K. Upadhyay, A. Mattevi, Molecular and mechanistic properties of the membrane-bound mitochondrial monoamine oxidases, Biochem. (Mosc.) 48 (2009) 4220–4230.
[11] C. Binda, J. Wang, L. Pisani, C. Caccia, A. Carotti, P. Salvati, D.E. Edmondson, A. Mattevi, Structures of human monoamine oxidase B complexes with selective noncovalent inhibitors: safinamide and coumarin analogs, J. Med. Chem. 50 (2007) 5848–5852.
[12] J. Kirchmair, S. Distinto, D. Schuster, G. Spitzer, T. Langer, G. Wolber, Enhancing drug discovery through in silico screening: strategies to increase true positives retrieval rates, Curr. Med. Chem. 15 (2008) 2040–2053.
[13] W.J. Geldenhuys, A.S. Darvesh, M.O. Funk, C.J. Van der Schyf, R.T. Carroll, Identification of novel monoamine oxidase B inhibitors by structure-based virtual screening, Bioorg. Med. Chem. Lett. 20 (2010) 5295–5298.
[14] F. Chimenti, D. Secci, A. Bolasco, P. Chimenti, A. Granese, S. Carradori, E. Maccioni, M.C. Cardia, M. Yanez, F. Orallo, S. Alcaro, F. Ortuso, R. Cirilli, R. Ferretti, S. Distinto, J. Kirchmair, T. Langer, Synthesis, semipreparative HPLC separation, biological evaluation, and 3D-QSAR of hydrazothiazole derivatives as human monoamine oxidase B inhibitors, Bioorg. Med. Chem. 18 (2010) 5063–5070.
[15] G.H. Braun, D.M.M. Jorge, H.P. Ramos, R.M. Alves, V.B. da Silva, S. Giuliatti, S.V. Sampaio, C.A. Taft, C. Silva, Molecular dynamics, flexible docking, virtual screening, ADMET predictions, and molecular interaction field studies to design novel potential MAO-B inhibitors, J. Biomol. Struct. Dyn. 25 (2008) 347–355.
[16] K. Boppana, P.K. Dubey, S. Jagarlapudi, S. Vadivelan, G. Rambabu, Knowledge based identification of MAO-B selective inhibitors using pharmacophore and structure based virtual screening models, Eur. J. Med. Chem. 44 (2009) 3584–3590.
[17] H. Kubinyi, Similarity and dissimilarity: a medicinal chemist's view, perspect, Drug Discov. 9-11 (1998) 225–252.
[18] C.G. Wermuth, Selective optimization of side activities: another way for drug discovery, J. Med. Chem. 47 (2004) 1303–1314.
[19] M. Yáñez, N. Fraiz, E. Cano, F. Orallo, Inhibitory effects of cis- and trans-resveratrol on noradrenaline and 5-hydroxytryptamine uptake and on monoamine oxidase activity, Biochem. Biophys. Res. Commun. 344 (2006) 688–695.
[20] H. Berman, K. Henrick, H. Nakamura, Announcing the worldwide protein data bank, Nat. Struct. Biol. 10 (2003) 980.
[21] Molecular Operating Environment (MOE), Chemical Computing Group, Inc, Montreal, 2008, 10.
[22] C. Barillari, J. Taylor, R. Viner, J.W. Essex, Classification of water molecules in protein binding sites, J. Am. Chem. Soc. 129 (2007) 2577–2587.
[23] N. Huang, B.K. Shoichet, Exploiting ordered waters in molecular docking, J. Med. Chem. 51 (2008) 4862–4865.
[24] M. Catto, O. Nicolotti, F. Leonetti, A. Carotti, A.D. Favia, R. Soto-Otero, E. Mendez-Alvarez, A. Carotti, Structural insights into monoamine oxidase inhibitory potency and selectivity of 7-substituted coumarins from ligand- and target-based approaches, J. Med. Chem. 49 (2006) 4912–4925.
[25] L. Novaroli, A. Daina, E. Favre, J. Bravo, A. Carotti, F. Leonetti, M. Catto, P.A. Carrupt, M. Reist, Impact of species-dependent differences on screening, design, and development of MAO-B inhibitors, J. Med. Chem. 49 (2006) 6264–6272.
[26] F. Chimenti, E. Maccioni, D. Secci, A. Bolasco, P. Chimenti, A. Granese, O. Befani, P. Turini, S. Alcaro, F. Ortuso, R. Cirilli, F. La Torre, M.C. Cardia, S. Distinto, Synthesis, molecular modeling studies, and selective inhibitory activity against monoamine oxidase of 1-thiocarbamoyl-3,5-diaryl-4,5-dihydro-(1*H*)-pyrazole derivatives, J. Med. Chem. 48 (2005) 7113–7122.
[27] C. Binda, F. Hubalek, M. Li, Y. Herzig, J. Sterling, D.E. Edmondson, A. Mattevi, Crystal structures of monoamine oxidase B in complex with four inhibitors of the *N*-propargylaminoindan class, J. Med. Chem. 47 (2004) 1767–1774.
[28] GRID, in, Molecular Discovery Ltd., Pinner, Middlesex, UK.
[29] P.J. Goodford, A computational procedure for determining energetically favorable binding sites on biologically important macromolecules, J. Med. Chem. 28 (1985) 849–857.
[30] R.C. Wade, Solvation of the active site of cytochrome P450-cam, J. Comput. Aided Mol. Des. 4 (1990) 199–204.
[31] R.H. Henchman, J.A. McCammon, Structural and dynamic properties of water around acetylcholinesterase, Protein Sci. 11 (2002) 2080–2090.
[32] G.J. Kleywegt, M.R. Harris, J.-y. Zou, T.C. Taylor, A. Wahlby, T.A. Jones, The Uppsala electron-density server, Acta Crystallogr. Sect. D: Biol. Crystallogr. 60 (2004) 2240–2249.
[33] P. Emsley, K. Cowtan, Coot: model-building tools for molecular graphics, Acta Crystallogr. Sect. D: Biol. Crystallogr. 60 (2004) 2126–2132.
[34] Schrödinger Suite, in, Schrödinger, LLC, New York, NY, USA.
[35] W. Sherman, T. Day, M.P. Jacobson, R.A. Friesner, R. Farid, Novel procedure for modeling ligand/receptor induced fit effects, J. Med. Chem. 49 (2006) 534–553.
[36] R.T. Kroemer, A. Vulpetti, J.J. McDonald, D.C. Rohrer, J.-Y. Trosset, F. Giordanetto, S. Cotesta, C. McMartin, M. Kihlen, P.F.W. Stouten, Assessment of docking poses: interactions-based accuracy classification (IBAC) versus crystal structure deviations, J. Chem. Inf. Comput. Sci. 44 (2004) 871–881.
[37] D. Yusuf, A.M. Davis, G.J. Kleywegt, S. Schmitt, An alternative method for the evaluation of docking performance: RSR vs RMSD, J. Chem. Inf. Model. 48 (2008) 1411–1422.
[38] P. Kallblad, R.L. Mancera, N.P. Todorov, Assessment of multiple binding modes in ligand–protein docking, J. Med. Chem. 47 (2004) 3334–3337.
[39] W.L. Jorgensen, J. Chandrasekhar, J.D. Madura, R.W. Impey, M.L. Klein, Comparison of simple potential functions for simulating liquid water, J. Chem. Phys. 79 (1983) 926–935.
[40] D.A. Gibson, E.A. Carter, Time-reversible multiple time scale ab initio molecular dynamics, J. Phys. Chem. 97 (1993) 13429–13434.
[41] J.P. Ryckaert, G. Ciccotti, H.J.C. Berendsen, Numerical integration of the cartesian equations of motion of a system with constraints: molecular dynamics of *n*-alkanes, J. Comput. Phys. 23 (1977) 327–341.
[42] T. Darden, D. York, L. Pedersen, Particle mesh Ewald: an N.log(N) method for Ewald sums in large systems, J. Chem. Phys. 98 (1993) 10089–10092.
[43] W. Humphrey, A. Dalke, K. Schulten, VMD: visual molecular dynamics, J. Mol. Graph. 14 (1996) 33–38, 27–38.
[44] Desmond Molecular Dynamics System, D.E Shaw Research, New York, NY, 2008.
[45] D.E. Edmondson, C. Binda, A. Mattevi, Structural insights into the mechanism of amine oxidation by monoamine oxidases A and B, Arch. Biochem. Biophys. 464 (2007) 269–276.
[46] C. Binda, M. Li, F. Hubálek, N. Restelli, D.E. Edmondson, A. Mattevi, Insights into the mode of inhibition of human mitochondrial monoamine oxidase B

from high-resolution crystal structures, Proc. Natl. Acad. Sci. U. S. A. 100 (2003) 9750–9755.
[47] C. Binda, F. Hubálek, M. Li, D.E. Edmondson, A. Mattevi, Crystal structure of human monoamine oxidase B, a drug target enzyme monotopically inserted into the mitochondrial outer membrane, FEBS Lett. 564 (2004) 225–228.
[48] D.E. Edmondson, A. Mattevi, C. Binda, M. Li, F. Hubalek, Structure and mechanism of monoamine oxidase, Curr. Med. Chem. 11 (2004) 1983–1993.
[49] G. Wolber, T. Langer, LigandScout: 3-D pharmacophores derived from protein-bound ligands and their use as virtual screening filters, J. Chem. Inf. Model. 45 (2005) 160–169.
[50] C.A. Lipinski, F. Lombardo, B.W. Dominy, P.J. Feeney, Experimental and computational approaches to estimate solubility and permeability in drug discovery and development settings, Adv. Drug Delivery Rev. 46 (2001) 3–26.
[51] W.L. Jorgensen, E.M. Duffy, Prediction of drug solubility from structure, Adv. Drug Delivery Rev. 54 (2002) 355–366.
[52] F. Chimenti, E. Maccioni, D. Secci, A. Bolasco, P. Chimenti, A. Granese, S. Carradori, S. Alcaro, F. Ortuso, M. Yáñez, F. Orallo, R. Cirilli, R. Ferretti, F. La Torre, Synthesis, stereochemical identification, and selective inhibitory activity against human monoamine oxidase-B of 2-methylcyclohexylidene-(4-arylthiazol-2-yl)hydrazones, J. Med. Chem. 51 (2008) 4874–4880.